Effect of Physical Nonlinearity on Local Buckling in Sandwich Beams††

VITALY KOISSIN*
Department of Metallurgy and Materials Engineering, Katholieke Universiteit Leuven, B-3001 Heverlee, Belgium

ANDREY SHIPSHA
Inspecta Technology AB, Box 30100, S-104 25 Stockholm, Sweden

VITALY SKVORTSOV
Department of Strength of Materials, State Marine Technical University, 198 262 St. Petersburg, Russia

ABSTRACT: This article deals with experimental, theoretical, and FE characterization of the local buckling in foam-core sandwich beams. In the theoretical approach, this phenomena is considered in a periodic formulation (unbounded wrinkle wave); a nonlinear stress–strain response of the face material is accounted for. In the FE approach, nonlinearity of the core material is also modeled. Full-field strain measurement is employed in the tests showing that the commonly used edgewise compression set-up can cause premature waviness of the faces, and therefore, nonlinear local deformations in the core layer.

KEY WORDS: sandwich structure, wrinkling, local buckling, modeling.

INTRODUCTION

THE WRINKLING (LOCAL BUCKLING) problem is an important part of the sandwich design, since the core layer provides a limited support for the in-plane compressed face sheets. This has been investigated in many studies, and a number of experimental findings and theoretical approaches appeared, e.g., [1–5]. The known solutions usually assume an explosive (bifurcation type) and unbounded propagation of the wrinkle waviness and

*Author to whom the correspondence should be addressed. E-mail: vitaly@kth.se
††This publication is dedicated to the memory of Prof. Vitaly Skvortsov (27.01.1958–26.09.2008) who greatly helped to give birth to the scientific way of the authors.
Figures 1–14, A1 and A2 appear in color online: http://jsm.sagepub.com

1099-6362/10/04 0477–18 $10.00/0 DOI: 10.1177/1099636209104521

a purely elastic behavior of the core material. The face sheet material is also often considered as ideally elastic. However, many materials (polymer composites, metals, etc.) exhibit a nonlinear deformation prominent under high stresses. The foam materials can also show a nonlinear response even at small strains. Finally, the local buckling usually does not occur simultaneously on the entire sandwich panel. All these features can cause the failure onset at a significantly lower load than that predicted by a linear-elastic model [1,4].

In this article, the local buckling of a typical foam-core sandwich is studied under uniaxial edgewise compression. The test set-up is shown to produce a complex stress–strain field in the core layer. Due to the nonlinear core material response, this effect results in a premature failure that can adequately be predicted only using an FE model.

EXPERIMENTAL

The object of study are straight beams ($47 \times 270\,mm^2$ in-plane dimension) comprised of thick Rohacell WF51 foam core and relatively thin transversely quasi-isotropic faces. The latter is made of four layers (symmetric lay-up) of E-glass noncrimp fabric impregnated with vinylester resin. Basic material data (the Young's modulus E, ultimate stress, σ_{ult}, τ_{ult}, and strain, ε_{ult}, γ_{ult}) are listed in Table 1. The Poisson's ratio, ν, is either estimated by the laminate theory or taken from the core manufacturer's data sheet [6]. Figures 1 and 2 show typical load curves and tangent moduli (derived by differentiation of the curves) of these materials under a quasi-static uniaxial loading. Large drop in the tangent moduli prior to the failure is seen in Figure 2, especially for the compressed foam material.

Standard Procedure

The edgewise compression tests are performed according to ASTM C364-94. The specimen edges are reinforced with 15 mm long tabs made of the

Table 1. Basic mechanical properties of the sandwich constituents (tension/compression).

Material	Thickness (mm)	E (MPa)	ν	ε_{ult} (%)	σ_{ult} (MPa)	γ_{ult} (grad)	τ_{ult} (MPa)
GFRP	2.4	24540[b]	0.25	2.2[a]/1.4[b]	295[a]/291[b]	–	–
WF51	50	85[c]	0.32	3.3[d]/2.3[c]	1.42[d]/0.90[c]	1.2[e]	0.5[e]

[a]ASTM D 638M, [b]ASTM D 3410, [c]ASTM D 1623-78 (out-of-plane of the foam block), [d]ASTM D 3039 (in-plane of the foam block), [e]ASTM C 273 (in-plane of the foam block).

same laminate as the face sheets and glued at their outer surfaces. Then, the edges are milled to ensure that they are flat and parallel. The specimens are compressed between two rigid plates at the cross-head displacement rate of 2 mm/min. Series of 10 specimens is tested.

A full-field displacement registration equipment (one digital camera with 1 fps picture frequency and Limess software) is used for several tests. Figure 3 shows a typical transversal strain field observed prior to the failure.

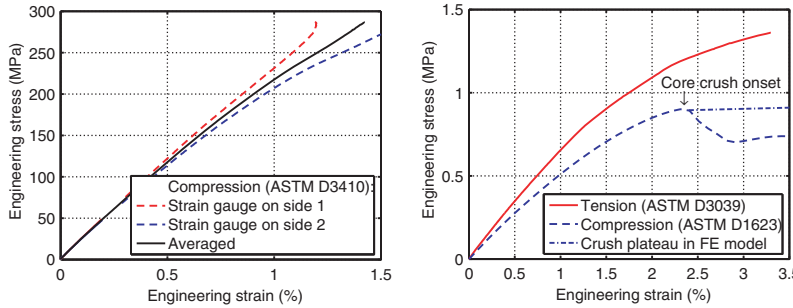

Figure 1. *Stress–strain curves for GFRP (left) and WF51 (right) under uniaxial loading.*

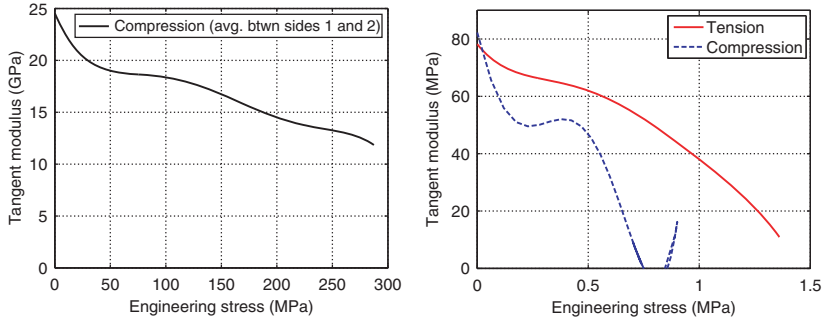

Figure 2. *Tangent moduli for GFRP (left) and WF51 (right) under uniaxial loading. Fitted with the fifth order polynomials, since the original data show a large scatter.*

Figure 3. *Typical strain field (ε_y) in the core prior to the failure. Undeformed coordinate system.*

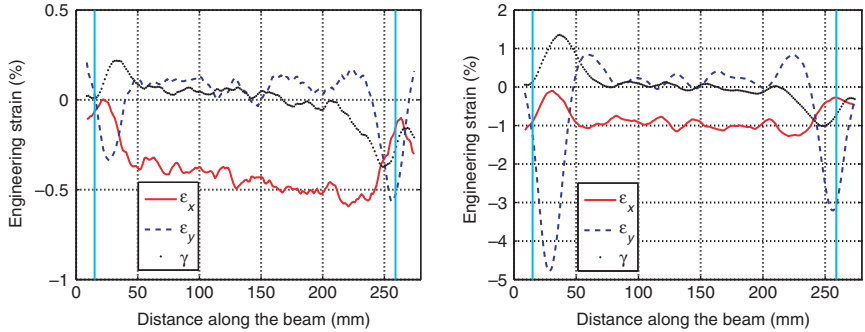

Figure 4. *Typical distribution of strains at the face–core interface (bottom face in Figure 3): step #51 (left) and #102 (right). Vertical lines indicate ends of the tabs.*

It is seen that the core undergoes a significant local deformation due to the face sheet waviness. This waviness appears already at the early loading stage, obviously due to (1) a load eccentricity (because of tabs) and (2) self-fixation of the edges at the loading plates that results in a slight swell of the specimen (because of the Poisson's effect). In principle, the first difficulty can be overcome by gluing extra tabs into the core underneath the face sheets, section 'Modified Procedure'. The second difficulty seems to be an inherent property of this standard test, since the friction inevitably prevents free transversal displacements of the specimen edges.

Figure 4 shows typical strain distributions along the face–core interface (at about 1 mm distance below the interface) for two loading stages. Particularly, Figure 4 (right) shows the strain components measured under the bottom face in Figure 3 (i.e., less than 1 s before the failure). Data shown in Figure 4 (left) are measured at the same line but much earlier (under approximately 1/2 of the ultimate load). Both plots exhibit waviness having prominent maximums near the tabs. At the moment of failure, the maximal compressive strain underneath the face–core interface is about 4% that is two times more than the yield strain typical for this foam grade, Table 1. Corresponding inward transversal displacements are about 0.6–0.8 mm. The tensile strain in the adjacent bulges approaches 1%; the maximal outward displacement is about 0.4–0.5 mm. Taking into account the nonlinear material response, Figure 1 (right), it is obvious that the supporting effect of the core layer decreases or even vanishes (due to the core crushing in compression) in these local areas.

Figure 5 (left) shows progression of several strain maximums (compressive and tensile) during the loading. The strains are measured and averaged within small circles near the bottom face as shown in Figure 3. The first and second maximums show almost constant strain rate until a certain moment,

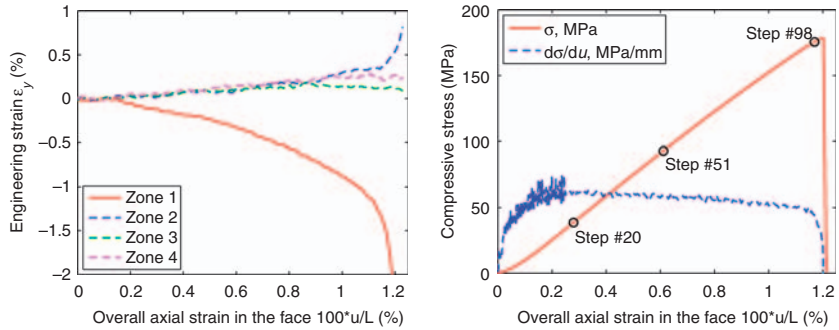

Figure 5. *Typical growth of the max. strain in the core (left) and typical load–displacement response (right, σ is given by Equation (1)) under edgewise compression. L is the beam length; u is the edge displacement.*

Table 2. Ultimate strength (σ_{ult}, MPa): test data vs. theoretical and FE predictions.

Test data	All linear-elastic		Nonlinear-elastic face		All nonlinear-elastic
Equation (1)	Equation (2)	FE	Equation (3)	FE	FE
168.3–192.4	317	344[a]/378[b]/378[c]	280	293[a]/314[b]/320[c]	217[a]/234[b]/275[c]

[a]Face as 1D elements, [b]face as 2D elements, [c]extra tabs and face as 2D elements.

when it increases suddenly. This can be attributed to the local buckling onset. The third and fourth maximums do not show such a behavior. Thus, the buckling is localized near the tabs and, in spite of a continuous waviness of face sheets, does not occur in the central part of the specimen, obviously due to almost intact (stiffer) support of the core layer. The face sheet debonding apparently starts in the second zone, most likely by a shear or tensile fracture of the foam material at the face–core interface.

The load curve (load cell signal vs. edge displacement), especially after its differentiation as shown in Figure 5 (right), can also be an indicator of the local buckling onset. It is seen that, after a short period of the clearance adjustment, the overall stiffness culminates in step #20 and then decreases gradually by about 25%. This effect should be attributed to a gradually increasing face sheet waviness as well as to a nonlinear behavior of the face and core materials. At step #98, the stiffness starts to degrade rapidly. This moment coincides with the local buckling onset seen in Figure 5 (left).

The test data are given in Table 2 in comparison with the theoretical and FE results discussed below. The ultimate stress is used, because it differs very little from the buckling onset value. Since the in-plane stiffness of the

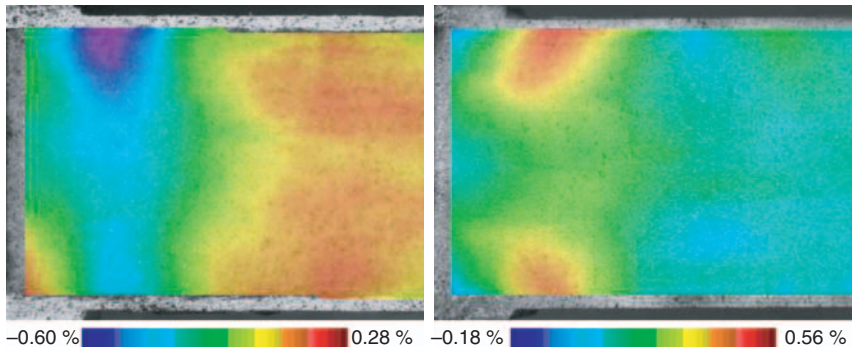

Figure 6. *Typical ε_y strain field in the core at step #60 for standard (left) or modified (right) specimen. Detail. Undeformed coordinate system.*

laminate is much larger than that of the core layer, the compressive stress in the face sheet is calculated as:

$$\sigma = \frac{P}{2h_f b}, \tag{1}$$

where P is the total load, h_f is the face thickness, and b is the beam width.

Modified Procedure

The modified specimen is manufactured by cutting gaps in the core under the face sheets and gluing there extra tabs (of the same size and material as the 'outer' tabs). Only one specimen is tested; the test procedure is identical to the one used before. Unfortunately, the overall bending occurs due to a slight initial curvature, and thus the obtained ultimate strength may not be taken into consideration. Nevertheless the strain distribution demonstrates that the modified configuration allows to eliminate the inward face dent and core crushing near the tabs. This is seen in Figure 6 (right); the image on the left shows the same area of interest in a standard specimen.

THEORETICAL

Consider static bending of an infinite beam (which represents the face sheet) having thickness h_f and bonded to an isotropic half-plane (which represents an infinitely thick core layer). The beam is axially compressed by a 'dead' force σh_f (per unit width). The face sheet is assumed to be thin, nonstretchable, and to keep the straight form of equilibrium up to the

critical state. Thus, there is no difference between displacements at its midplane and at the face–core interface, and no influence of the interfacial shear stress. As a first approximation, both the face and core materials are considered as ideally linear-elastic. Using the thin plate Kirchoff–Love theory for the face and Lamé equations for the core, the critical (in the Euler's sense) stress for this model is [7]:

$$\sigma_{ult} = \frac{3}{\sqrt[3]{4}} \frac{x_n}{h_f} E_1, \quad x_n^3 = \frac{D_f}{E_1}, \quad D_f = \frac{E_f h_f^3}{12},$$
$$E_1 = \frac{2E_c}{(1+\nu_c)(3-\nu_c)}, \quad l = \pi\sqrt[3]{2}x_n \tag{2}$$

where D_f is the flexural rigidity of the face sheet, E_1 is the reduced elastic modulus of the core layer (plane stress state is assumed), and l is the natural wavelength. The refined approach accounting for a finite core thickness is given in the Appendix.

Using Equation (2) and elastic properties from Table 1, the critical stress is easily calculated. However, its value exceeds the average test data (175.7 MPa) in 80%, Table 2. The natural wavelength is estimated to be about 33 mm that also disagrees with Figure 4 (about 17 mm).

Of course, a better approach is to account for the nonlinear behavior of the face sheet material. For example, the reduced modulus of elasticity (called also the von Kármán's modulus) can be used. In the present case of a rectangular cross-section its reads as:

$$E_r(\sigma) = \frac{4E_f E_t(\sigma)}{\left(\sqrt{E_f} + \sqrt{E_t(\sigma)}\right)^2}, \tag{3}$$

where E_t is the tangent modulus, Figure 2 (left). The reduced modulus theory assumes that a stress release occurs on the convex side of the beam simultaneously with the buckling onset. For a short-length wrinkle wave the use of Equation (3) is even conservative, since certain portions of the face sheet undergo mainly rotation with a minor bending and thus have a stress release on both sides. This is because the wrinkled face sheet is less shortened than in the case of an ideally uniaxial deformation. Therefore, the 'correct' critical stress will lie somewhere above the value calculated using the reduced modulus [8,9].

After substitution of Equation (3), Equation (2) becomes nonlinear and requires a numerical procedure. Solution is given in Table 2. As can be seen, the reduced modulus theory gives more realistic estimation of the critical stress if compare with the purely elastic solution; however, the predicted

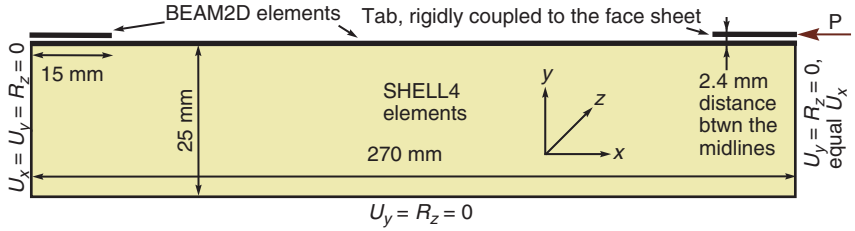

Figure 7. *Schematic of the FE model, not scaled.*

value is still 60% higher than the experimental one. The natural wavelength is estimated to be about 29 mm that is also still not realistic.

Thus, the face sheet material nonlinearity has important but not primary destabilizing influence on the structure. To approach a more accurate solution, it is necessary to account for localization of the face sheet bending and for local nonlinear deformation of the core material, which are observed in the experimental study. Obviously this cannot be achieved analytically, and an FE analysis should thus be applied.

FE ANALYSIS

The FE package COSMOSM is used. Since the core layer is thick, and the strains decay rapidly through its thickness, Figure 3, only one face sheet and half of the core thickness are modeled. Schematic of the model with applied boundary conditions is shown in Figure 7.

Simplistic Model: 1D Elements for the Face Sheet

The core is meshed as a rectangular domain with 4-node isotropic shell elements (SHELL4). The face and tabs are meshed with 2-node beam elements (BEAM2D).The model is composed of 10 elements through the core and 108 elements lengthwise, i.e., a $2.5 \times 2.5\,\text{mm}^2$ mesh is created. The tabs have the same mesh density and are coupled node-to-node to the face, enforcing the two nodes to rotate and move by the same amount.

A conservative compressive load (concentrated force) is applied at the edge of one of the tabs. Actually, it should be applied somewhere in between the tab midplane and the face midplane, or applied in two portions at both mid-lines. The used way is a conservative simplification resulting in a larger load eccentricity.

The linear-elastic analysis is performed first. The buckling mode (only the first mode is considered here) is shown in Figure 8 (top); a slight nonsymmetry is seen which can be attributed to a limited length of

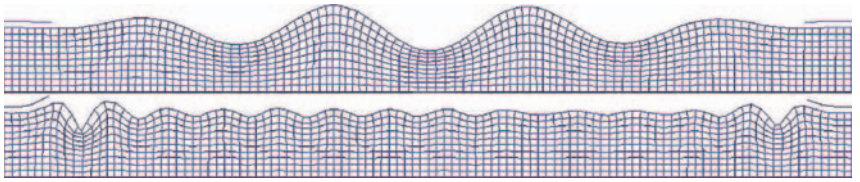

Figure 8. *Buckling modes: linear-elastic face and core (top) or nonlinear elastic face and linear-elastic core (bottom). Geometrically linear solutions.*

the model. The critical stress agrees well with the theoretical estimation by Equation (2), Table 2; the difference does not exceed 10%. The wavelength is about 30 mm that is also close to the theoretical results.

A more refined model accounts for the nonlinear elastic response of the face sheet material, Figure 1 (left). In the software, the nonlinear elastic model relies on the assumption of proportional loading, when components of the stress tensor vary monotonically in a constant ratio to each other. Then, the total strain vector is used to compute the effective strain to obtain the current position at the defined stress–strain curve [10].

Result of a geometrically linear FE analysis is given in Table 2 and shows a minor (about 5%) discrepancy with the theoretical value calculated using the reduced modulus theory. The buckling mode (again nonsymmetric with respect to the center) is shown in Figure 8 (bottom). However, the wavelength is about two times smaller than the theoretical one (12 mm vs. 29 mm). The reason for this effect is not yet clear for the authors.

Finally, nonlinear response of the core material is also introduced into the FE model, according to Figure 1 (right). The same nonlinear elastic material model is used as for the face sheet; the foam crush plateau is modeled as almost horizontal line producing very low tangent modulus, see the dash-and-dot line in Figure 1 (right). Geometrically nonlinear analyses are performed to calculate the equilibrium displacement solutions for a number of given loads, by using the modified Newton–Raphson method under the load control.

The deformed shape and strain fields are shown in Figure 9 for load step #18 at which, as proved below, the local buckling occurs. Comparison with the full-field measurements, Figure 3, reveals a good agreement of the strain pattern. However, the FE analysis overestimates the maximal strains by a factor of 2. This can be due to (1) significantly increased, if compare to a real specimen, load eccentricity and (2) localization of the core 'crushing' in the elements adjoining the face sheet (in a real specimen, the foam cells are filled with the resin at the interface and thus have a smoother strain field).

Figure 10 (left) shows growth of the maximal strains in the core during the loading. It is seen that the tensile strain under the bulge (that corresponds to

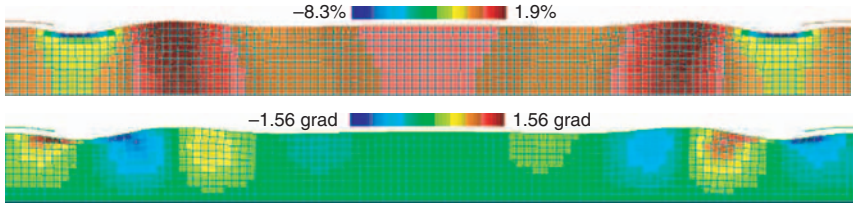

Figure 9. *Strain fields at the load step #18: transversal, ε_y, (top) and shear, γ, (bottom). Nonlinear elastic face and core, geometrically nonlinear solution. The deformed shape is scaled by a factor of 5.*

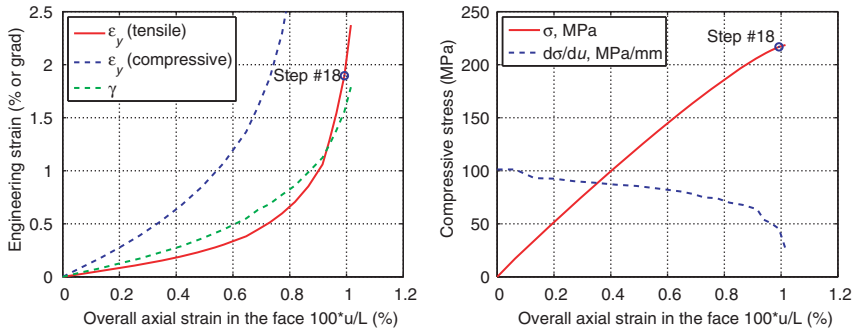

Figure 10. *Growth of the max. strains in the core (left) and load–displacement response (right) in the nonlinear FE analysis. L is the beam length; u is the edge displacement.*

zone #2 in Figure 3) cannot initiate the failure, since the ultimate value (3.3%, Table 1) is not reached. The model can most likely fail by the shear fracture, since the maximal shear stress exceeds the ultimate value of 1.2 grad. But these are very rough speculations hardly applicable to the real sandwich beams, because the shear strength data are obtained on large foam specimens, which failed due to a stress concentration [11]. Last but not the least, the used rheological model (nonlinear elasticity with proportional strain growth) and uniaxial test data cannot provide a quantitatively correct results for the strain fields.

The load curve is shown in Figure 10 (right), along with the stiffness function. They generally resemble Figure 5 (right), although the FE model produces a stiffer response. As in the real specimens, the stiffness degradation accelerates at a certain moment (step #18), which may be considered as the local buckling onset. The corresponding stress, Table 2, is close to the upper limit of the test data, the difference is only 13%. Taking into account imperfections existing in the real specimens and simplifications introduced in the FE analysis, such a result is wholly satisfactory.

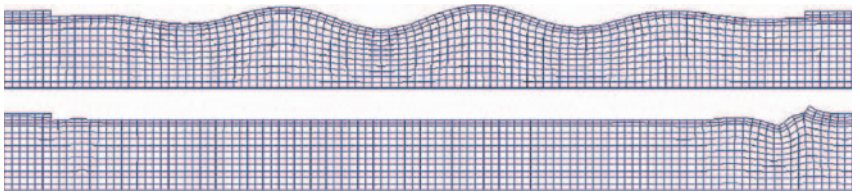

Figure 11. *Buckling modes: linear-elastic face and core (top) or nonlinear elastic face and linear-elastic core (bottom). Geometrically linear solutions. The face sheet and tabs are meshed with* SHELL4 *elements.*

Refined Model: 2D Elements for the Face Sheet and Tabs

In the refined approach the face sheet and tabs are modeled using two SHELL4 elements through the thickness of each of them. Then there is no need to couple the tab and face nodes. The load is applied in three equal portions at $y = 0$ (face–core interface), $y = h_f$ (face–tab interface) and $y = 2h_f$ (top of the tab). The transversal Young's modulus is estimated with the Chamis' theory (10.7 GPa, taking typical E-glass stiffness of 72 GPa and matrix stiffness of 3.1 GPa). The rest of the model stays the same as shown in Figure 7.

In the geometrically linear analysis, the behavior generally resembles the previous case, although the ultimate loads are a little higher, Table 2, and the eigen modes are more nonsymmetric, Figure 11. The latter is especially prominent for the model with nonlinear face and linear core responses; its buckling is now confined near the right (loaded) tab. This is obviously due to a strain localization that cannot be attained with simplistic BEAM2D elements but easily appears when SHELL4 elements are used for the face sheet.

The deformed shape and strain fields for the model with nonlinear response of both materials are very similar to these shown in Figure 9. At the buckling onset, the strain maximums in the core are larger: $-13.3\% < \varepsilon_y < 3.1\%$ and $|\gamma| < 2.72$ grad (although the ultimate state is now reached later, at step #24; for step #18 the strains are smaller than for the case with BEAM2D elements). The load curve and the strain growth response are also similar to Figure 10.

Refined Model: Modified Variant

To model the modified test set-up, 'Modified Procedure' section, the same FE model described above is used. The only difference is in additional tabs inserted under the face sheet (with the same dimensions, mesh, and properties as the 'outer' ones). The load is now divided between four points; the fourth component is applied at $y = -h_f$ ('inner' tab-core interface).

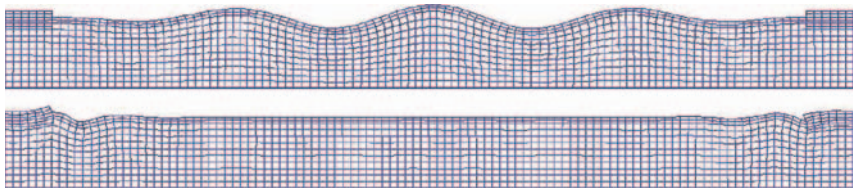

Figure 12. *Buckling modes: linear-elastic face and core (top) or nonlinear elastic face and linear-elastic core (bottom). Geometrically linear solutions. The face sheet and tabs are meshed with SHELL4 elements. Case with additional 'inner' tabs.*

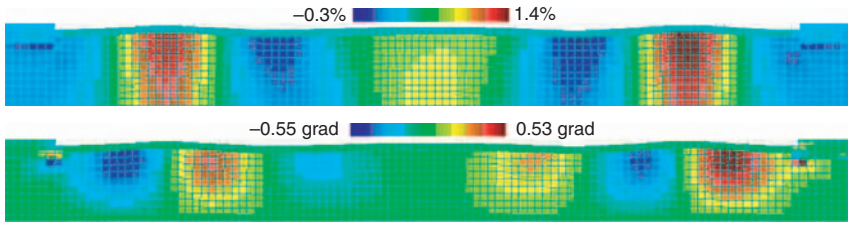

Figure 13. *Strain fields at the load step #35: transversal, ε_y, (top) and shear, γ, (bottom). Nonlinear elastic face and core, geometrically nonlinear solution. The deformed shape is scaled by a factor of 5. The face sheet and tabs are meshed with SHELL4 elements. Case with additional 'inner' tabs.*

As expected, the geometrically linear analysis yields almost the same ultimate loads, Table 2. The eigen modes are shown in Figure 12. For the purely linear case the mode returns the symmetry, while it becomes antisymmetric for the case of the nonlinear face and linear core material responses.

Figure 13 shows the deformed shape and strain fields for the model with nonlinear behavior of both materials, prior to the local buckling (when the solution becomes unstable). Comparison with Figure 9 shows that the modified model gives more mild strains. The most important point is that the core crushing is not reached, since no dent occurs near the tabs. Thus the local bending of the face sheet cannot significantly affect the ultimate load.

There is also a stress concentration at the tips of the 'inner' tabs but this obviously does not play a role for the local buckling and can be eliminated by using a smoother tab profile, instead of the right angle. The experimental observations do not show this strain gradient, Figure 6 (right). In the FE model the outward face bending occurs at about 30 mm distance from the tabs, while it happens at about 10 mm distance in the real specimen, Figure 6 (right). The reason for this discrepancy is not yet clear.

Figure 14 shows growth of the maximal strains in the core during the loading as well as the load curve and the stiffness function. With the

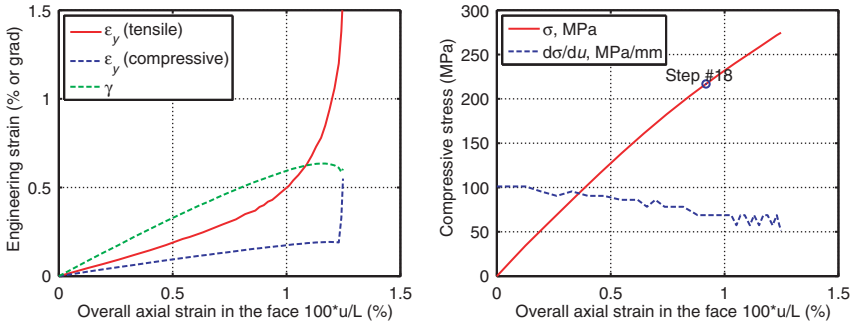

Figure 14. *Growth of the max. strains in the core (left) and load–displacement response (right) in the nonlinear FE analysis. L is the beam length; u is the edge displacement. The face sheet and tabs are meshed with* SHELL4 *elements. Case with additional 'inner' tabs.*

exception of the load curve, the general appearance is changed when compared with Figure 10. The rate of the stiffness degradation is almost constant up to the final load step; this indicates that the stability is lost close to the bifurcation manner. The same is seen for the strain responses shown in Figure 14 (left). The ultimate load (Table 2), approaches the analytical solution by Equation (3). This is a reasonable result, since the nonlinear effects mostly confine now within the face sheet.

CONCLUSIONS

The main results of this study can be outlined as

- the specimen configuration commonly used for the edgewise compression testing of sandwich beams has a load eccentricity due to the presence of tabs. This causes a local bending of the face sheet accompanying by a nonlinear deformation of the foam core. As a result, the buckling is localized, and the ultimate load can significantly be lower than that predicted by a linear stability analysis;
- therefore, for some combinations of the sandwich constituents, non-linearity of the face sheet and core materials can be very important for a correct prediction of the ultimate load. These effects can adequately be accounted for only in an FE analysis. It is demonstrated that the simplest uniaxial test data combined with a low-CPU FE model can provide a solution sufficient for the engineering purposes;
- a modified test specimen is proposed, with additional tabs glued under the faces. This configuration is proved to produce smaller local bending of the face sheets and, therefore, much lower local degradation of the core support. In this case the ultimate load significantly exceeds the one

attained with the standard specimen and approaches the theoretical estimation;
- the results can be improved by introducing more realistic rheological behavior and by using more complex test data (e.g., for multi-axial strain state) in the FE model, especially for the core material. Also, a better load application can be achieved by meshing the loading plates (and then solving the contact problem). Accounting for nonuniformity of the density distribution through-the-thickness of the foam core [11], can also provide a better solution.

ACKNOWLEDGMENTS

This study was done within the I-TOOL ('Integrated Tool for Simulation of Textile Composites') project funded by the European Commission. The authors are thankful to Prof. Stepan Lomov (Dept. MTM, Katholieke Universiteit Leuven, Belgium) for his interest to this study. Dr Dmitry Ivanov (ibid) is gratefully acknowledged for his help with the full-field strain measurements. Authors would also like to thank Mr Kris Van de Staey (ibid) for assistance with the mechanical testing.

APPENDIX: ELASTIC WRINKLING FOR A FINITE CORE THICKNESS

There are three modes of wrinkling mentioned as 'classic' ones in the literature, Figure A1. To obtain the critical stress, consider the static bending of a transversely isotropic face sheet (thickness h_f) bonded to an isotropic core layer (thickness h_c). Axial strain in the face as well as shear stress at the face-core interface are neglected. The governing equation for the face deflection, w_f, is given by the thin plate Kirchhoff theory as

$$D_f w_f(x)'''' + \sigma h_f w_f(x)'' = \frac{P}{2}\delta(x) + \sigma_{if}(x), \tag{A.1}$$

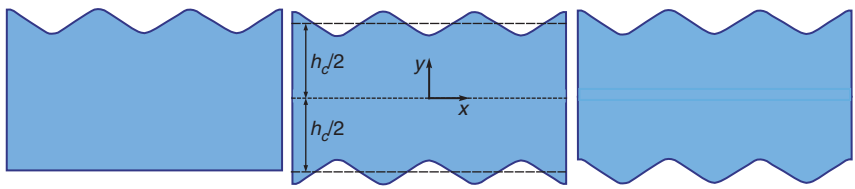

Figure A1. *Wrinkling modes: asymmetric, symmetric, and anti-symmetric.*

where $0 \le x \le \infty$, D_f is the bending stiffness, σh_f is the axial compressive load per unit width, δ is the Dirac delta-function, σ_{if} is the interfacial normal stress. Parameter P is a trial line load introduced at $x = 0$ to allow for the integral transforms technique employed below.

The Lamé equations are used for the core:

$$\begin{aligned} 2(1-\nu_c)w''_{yy} + (1-2\nu_c)w''_{xx} + u''_{xy} &= 0, \\ 2(1-\nu_c)u''_{xx} + (1-2\nu_c)u''_{yy} + w''_{xy} &= 0, \end{aligned} \tag{A.2}$$

where ν_c is the Poisson's ratio, $w \equiv w(x,y)$, $u \equiv u(x,y)$. Assuming symmetry with respect to x axis, this system is solved by means of Fourier integral transformation [12]. For symmetric functions (e.g., w and σ_{if}), the cosine transform is used:

$$\bar{f}(\omega) = \int_0^\infty f(x)\cos(\omega x)\mathrm{d}x, \quad f(x) = \frac{2}{\pi}\int_0^\infty \bar{f}(\omega)\cos(\omega x)\mathrm{d}\omega.$$

Analogously, the sine transformation is used for other functions (u, w'_x, etc.). After integration by parts, the transformed system (A.2) is:

$$\begin{aligned} 2(1-\nu_c)\bar{w}''_{yy} - (1-2\nu_c)\omega^2\bar{w} + \omega\bar{u}'_y &= 0, \\ 2(1-\nu_c)\omega^2\bar{u} - (1-2\nu_c)\bar{u}''_{yy} + \omega\bar{w}'_y &= 0, \end{aligned} \tag{A.3}$$

where $\bar{w} \equiv \bar{w}(\omega,y)$ and $\bar{u} \equiv \bar{u}(\omega,y)$. Thus the problem of solving the partial differential equations is reduced to that for the ordinary ones.

First consider the case when one of the faces (e.g., the bottom one, $y = -h_c/2$) undergoes no deflection, while another one, $y = h_c/2$, is allowed to buckle under the in-plane compression, Figure A1 (left). Then the boundary conditions are:

$$y = h_c/2 \colon w = w_f(x),\ u = 0, \quad y = -h_c/2 \colon w = 0,\ u = 0,$$

The solution for (A.3) is taken in the form:

$$\begin{aligned} \bar{w} &= \exp(\omega z)(a_1 + a_2\omega z) + \exp(-\omega z)(a_3 + a_4\omega z) \\ \bar{u} &= \exp(\omega z)(a_5 + a_6\omega z) + \exp(-\omega z)(a_7 + a_8\omega z). \end{aligned}$$

Omitting cumbersome calculations, relation between the images of the face deflection and normal interfacial stress reads as: ($\bar{\sigma}_{if} \equiv \bar{\sigma}_{if}(\omega)$,$\bar{w}_f \equiv \bar{w}_f(\omega)$)

$$\begin{aligned} \bar{\sigma}_{if} &= -E_1\omega F(\omega)\bar{w}_f, \\ F(\omega) &= \frac{\cosh(\omega h_c)\sinh(\omega h_c) + \psi\omega h_c}{\sinh^2(\omega h_c) - (\psi\omega h_c)^2} \end{aligned} \tag{A.4}$$

with (E_c is the Young's modulus of the core material):

$$E_1 = \frac{2\psi E_c}{(1+\nu_c)^2}, \quad \psi = \frac{1+\nu_c}{3-\nu_c} \quad \text{or}$$
$$E_1 = \frac{2\psi E_c(1-\nu_c)}{1+\nu_c}, \quad \psi = \frac{1}{3-4\nu_c}$$

for the plane stress or plane strain formulations, respectively.

Transformed Equation (A.1) is:

$$D_f \omega^4 \bar{w}_f - \sigma h_f \omega^2 \bar{w}_f = \frac{P}{2} + \bar{\sigma}_{if}. \tag{A.5}$$

Substitution of Equation (A.4) into Equation (A.5) gives the image:

$$\bar{w}_f = \frac{P/2}{D_f \omega^4 - \sigma h_f \omega^2 + E_1 \omega F(\omega)}. \tag{A.6}$$

Inverse transform of Equation (A.6) produces the original function:

$$w_f(x) = \frac{P}{\pi E_1} \int_0^\infty \frac{\cos(tx)\mathrm{d}t}{t^4 - kt^2 + tF(t)},$$

where $t = \omega x_n$ ($\omega h_c = t/\varepsilon$), $\varepsilon = x_n/h_c$, $k = \sigma h_f x_n^2/D_f$, $x_n = \sqrt[3]{D_f/E_1}$. The solution vanishes when the denominator becomes zero at minimal t. This occurs when:

$$t^3 - kt + F(t) = 0 \quad \text{and} \quad 3t^2 - k + F(t)'_t = 0.$$

In another form the critical value of the load parameter is:

$$k_{cr} = t^2 + \frac{F(t)}{t}, \quad \text{where } t \text{ is given by} \quad 2t^2 - F(t) + tF(t)'_t = 0. \tag{A.7}$$

Two ultimate cases correspond to an infinitely thick or very thin core layer:

$$F(\omega) \overset{\omega h_c \to \infty}{\longrightarrow} = 1, \quad F(\omega) \overset{\omega h_c \to 0}{\longrightarrow} = \frac{1}{\omega h_c (1-\psi)}.$$

The former case produces:

$$k_{cr} = \frac{3}{\sqrt[3]{4}} \quad \text{or} \quad \sigma_{cr} = \frac{3}{\sqrt[3]{4}} \frac{D_f}{h_f x_n^2} = \frac{3}{\sqrt[3]{4}} \frac{x_n}{h_f} E_1, \tag{A.8}$$

which is in agreement with Equation (2) used above, 'Theoretical' Section.

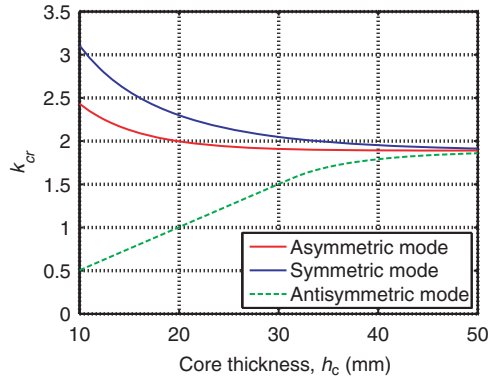

Figure A2. *Critical value of the load parameter k_{cr} vs the core thickness for different wrinkling modes shown in Figure A1. Elastic properties from Table 1 are used.*

The case of a symmetric deformation, Figure A1 (middle), is solved in a similar approach, with the following boundary conditions and functions:

$$y = \frac{\pm h_c}{2} : w = \pm w_f(x),$$
$$\bar{w} = a_1 \sinh(\omega z) + a_2 \omega z \cosh(\omega z),$$
$$\bar{u} = a_3 \cosh(\omega z) + a_4 \omega z \sinh(\omega z),$$

that yields:

$$F(\omega) = \frac{\cosh(\omega h_c) + 1}{\sinh(\omega h_c) - \psi \omega h_c}.$$

For the antisymmetric case, Figure A1 (right), the boundary conditions and general solution are:

$$y = \frac{\pm h_c}{2} : w = w_f(x),$$
$$\bar{w} = a_1 \sinh(\omega z) + a_2 \omega z \sinh(\omega z),$$
$$\bar{u} = a_3 \sinh(\omega z) + a_4 \omega z \cosh(\omega z),$$

which leads to:

$$F(\omega) = \frac{\cosh(\omega h_c) - 1}{\sinh(\omega h_c) + \psi \omega h_c}.$$

The critical value of k is again determined with Equation (A. 7), after $F(\omega)$ is transformed into $F(t)$ by replacing ωh_c for t/ε. The variation of k_{cr} vs. the core thickness is shown in Figure A2. It is seen that for the present case of $h_c = 50\,\text{mm}$ the difference between the critical stresses is negligibly small; they all approach the value of $3/\sqrt[3]{4}$ ($h_c = \infty$). Thus the simplest estimation (A.8) may be used.

REFERENCES

1. Stiftinger, M.A. and Rammerstorfer, F.G. (1997). On Face Wrinkling in Sandwich Shells – Theoretical and Experimental Investigations, *Thin-walled Structures*, **29**(1–4): 113–127.
2. Fleck, N.A. and Sridhar, I. (2002). End Compression of Sandwich Columns, *Composites Part A*, **33**: 353–359.
3. Fagerberg, L. (2003). Wrinkling of Sandwich Panels for Marine Applications, PhD Thesis, Department of Aeronautics & Vehicle Engineering, Royal Institute of Technology, Stockholm, Sweden.
4. Gdoutos, E.E., Daniel, I.M. and Wang, K.-A. (2003). Compression Facing Wrinkling of Composite Sandwich Structures, *Mechanics of Materials*, **35**(3–6): 511–522.
5. Birman, V. and Bert, C.W. (2004). Wrinkling of Composite-facing Sandwich Panels Under Biaxial Loading, *Journal of Sandwich Structures and Materials*, **6**: 217–237.
6. ROHACELL (1987). *Technical Manual*, Röhm GmbH, Darmstadt.
7. Koissin, V., Skvortsov, V. and Shipsha, A. (2007). Stability of the Face Layer of Sandwich Beams with Sub-interface Damage in the Foam Core, *Journal of Composite Structures*, **78**(4): 507–518.
8. Vol'mir, A.S. (1967). *Stability of Structures*, Nauka, Moscow [in Russian].
9. Bažant, Z.P. and Cedolin, L. (2003). *Stability of Structures: Elastic, Inelastic, Fracture, and Damage Theories*, Dover Publications Inc., New York.
10. Cosmos/M 2.0 User's Guide (1998).
11. Koissin, V. and Shipsha, A. Residual In-plane Mechanical Properties of Transversely Crushed Structural Foams, To appear in *Journal of Sandwich Structures and Materials*.
12. Sneddon, I.N. (1951). *Fourier Transform*, McGraw-Hill Book Co., NY.